MARCH 25 2026

4-Dimensional lung ultrasound imaging for lung surface motion estimation: an *in vivo* feasibility study

Federico Mento ; Chiara Zangrandi; Ziemowit Klimonda; Piotr Jarosik; Marcin Lewandowski; Libertario Demi

Proc. Mtgs. Acoust. 60, 020001 (2025)
https://doi.org/10.1121/2.0002275

Volume 60 http://acousticalsociety.org/

Sixth Joint Meeting

189th Meeting of the Acoustical Society of America and the Acoustical Society of Japan

Honolulu, Hawaii
1-5 December 2025

Biomedical Acoustics: Paper 2aBAa9

4-Dimensional lung ultrasound imaging for lung surface motion estimation: an *in vivo* feasibility study

Federico Mento and Chiara Zangrandi
Department of Information Engineering and Computer Science, University of Trento: Universita degli Studi di Trento Dipartimento di Ingegneria e Scienza dell'Informazione, Trento, 38123, ITALY; federico.mento@unitn.it; chiara.zangrandi@unitn.it

Ziemowit Klimonda, Piotr Jarosik and Marcin Lewandowski
us4us, Warsaw, POLAND; ziemowit.klimonda@us4us.eu; piotr.jarosik@us4us.eu; marcin@us4us.eu

Libertario Demi
Department of Information Engineering and Computer Science, University of Trento: Universita degli Studi di Trento Dipartimento di Ingegneria e Scienza dell'Informazione, Trento, 38123, ITALY; libertario.demi@unitn.it

Lung ultrasound (LUS) is nowadays widely spread in the clinical world. LUS analysis generally does not rely on the dynamics of LUS videos, being thus limited to the evaluation of specific LUS frames. Only rare LUS applications rely on dynamics, but without quantifying lung surface motion (LSM). For example, the presence of pneumothorax correlates with the absence of pleural sliding. Moreover, pleural sliding is assessed through the analysis of B-Mode LUS videos (3D data), which cannot guarantee PS to reliably represent LSM. Hence, in this study, for the first time, we evaluated the possibility to estimate LSM with 4-Dimensional (4D) LUS. Specifically, we assessed whether a velocity model based on functional ultrasound (fUS) applied to 4D LUS data can be used to differentiate normal breathing [NBr] (10-20 breaths per min [BPM]) and fast breathing [FBr] (40-60 BPM). Results showed how mean velocity for FBr equals 13.17 mm/s, corresponding to 1.88 times the mean velocity for NBr (7.01 mm/s), thus showing a variation consistent with the BPM change among NBr and FBr. Moreover, estimated velocities are within physiological range, proving, for the first time, the possibility to estimate LSM with 4D LUS.

Proceedings of Meetings on Acoustics, Vol. 60, 020001 (2026); https://doi.org/10.1121/2.0002275.

1. INTRODUCTION

Lung ultrasound (LUS) is a safe and effective imaging technique that is widely used in clinical settings. However, LUS data analysis is based on the visual interpretation of imaging patterns, as the presence of air does not enable the anatomical reconstruction of the lungs[1,2]. A way to overcome this main drawback is by implementing quantitative LUS solutions. Indeed, recent studies have been focusing on the characterization of imaging patterns by extracting quantitative features from LUS data[1]. Quantitative features demonstrated differentiating potential among different pathologies[1–5], highlighting the possibility of using them as relevant parameters during the diagnostic process. However, the proposed quantitative solutions focused mainly on the static aspect of LUS data[1,3,4], neglecting important information that might be found in the dynamics of LUS videos. For example, dynamic features that reflect the lung surface motion (LSM) might hold significant diagnostic potential.

A well-known imaging pattern that reflects LSM is pleural sliding. This pattern is defined as the lateral movement of the pleural line on B-mode LUS videos [3D (lateral dimension, axial dimension, and time) data][6]. To clarify, the intersection between the pleural plane (PPl) and the imaging plane is represented as the pleural line in the reconstructed B-Mode images [2D (lateral dimension and axial dimension) data]. Pleural sliding is thought to be caused by the sliding against each other of the two pleural layers[6], and is a relevant imaging pattern, as its absence indicates a pathological case, such as pneumothorax[7]. Despite its importance, the quantification of pleural sliding is still an open topic in research, and only few studies focus on it. Among these, the majority quantified this pattern in terms of amplitude[8–13]. Few methodologies have been proposed to estimate the velocity of pleural sliding (sliding velocity). Xiao et al.[14] and Briganti et al.[8] estimated this velocity by applying Doppler ultrasound, while Tzadok et al.[15] implemented a speckle tracking technique. Xiao et al.[14] and Tzadok et al.[15] reported velocity values within a physiological range (order of a few millimeters per second [mm/s]), whereas Briganti et al.[8] reported velocities on the order of tens of centimeters per second (cm/s).

Even though these studies provided some insightful results, the implementation of these techniques might not be suitable because their assumptions may not be valid in LUS data. For example, a fully formed speckle pattern cannot be assumed to be present on the pleural line. Moreover, they analyze cross-sectional 3D data (lateral dimension, axial dimension, and time), overlooking motion along the elevation dimension. This type of data could not guarantee a reliable representation of LSM, highlighting the need for 4D imaging. Beyond LUS application, other motion tracking approaches exist in ultrasound imaging (e.g., Kasai[16]), and they can be explored in future studies for comparison with the proposed approach.

The objective of this study is to estimate LSM velocity with a velocity model based on functional ultrasound (fUS) applied to 4D LUS. Specifically, we assess whether this feature can differentiate between normal breathing (NBr) and fast breathing (FBr). The breathing rates of NBr and FBr are approximately 10-20 breaths/min and 40-60 breaths/min.

The rest of the paper is structured as follows. In Section 2, the proposed methodology is explained. In Section 3, results are discussed. Finally, Section 4 summarizes conclusions and future work.

2. METHODOLOGY

A. DATASET

In this study, data were acquired from a healthy volunteer (protocol 2025-056 approved by the Ethical Committee for Research, University of Trento). The acquisition protocol involved two sessions with different types of breathing (NBr and FBr). The healthy volunteer was asked to breathe normally during the first session and to increase the breathing rate during the second session. In both sessions, the volunteer was scanned by placing the probe on the right anterior chest region, and a 5 seconds video was acquired.

A us4R-lite™ scanner (us4us, Varsaw, Poland) equipped with a Vermon row column array (RCA) 64+64 (3 MHz, bandwidth ~70%) probe (Vermon, Tours, France) was utilized for data acquisition. Radiofrequency (RF) 4D videos were acquired with a 4-angle plane wave compounding. A 3-MHz pulse (1 cycle) was used during transmission, and a sampling frequency of 65 MHz utilized in reception. To reconstruct 2x2x5 cm (along lateral, elevation, and depth dimensions) volume images, a volume rate (VR) of 40 Hz was utilized.

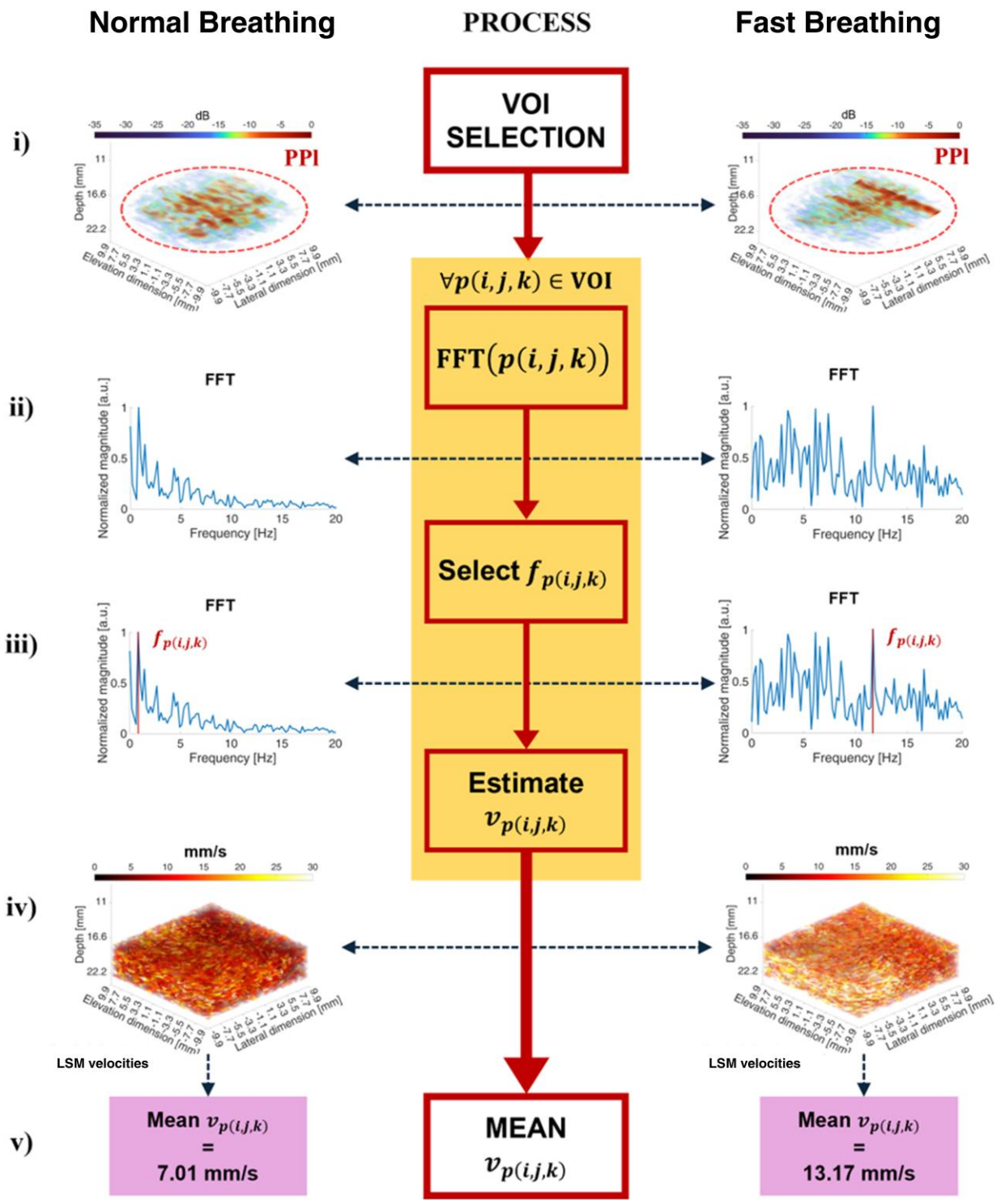

Figure 1. Estimation process of LSM velocity. The process pipeline is outlined in the center column of the figure. The corresponding outputs of each step of the pipeline are presented in the left column for Normal Breathing (NBr) and in the right column for Fast Breathing (FBr). The rows of the figure represent the five steps of the process. Row i) highlights the VOI selection, defined as to totally include the pleural plane (PPl). Row ii) reports some examples of FFT of slow-time intensity (STI) signals. Row iii) highlights the selection process of $f_{p(i,j,k)}$, identified as the maximum magnitude on the FFT. Row iv) shows the estimated $v_{p(i,j,k)}$. Each pixel of the reconstructed volume is color-coded according to its own velocity. Row v) reports the mean $v_{p(i,j,k)}$ values.

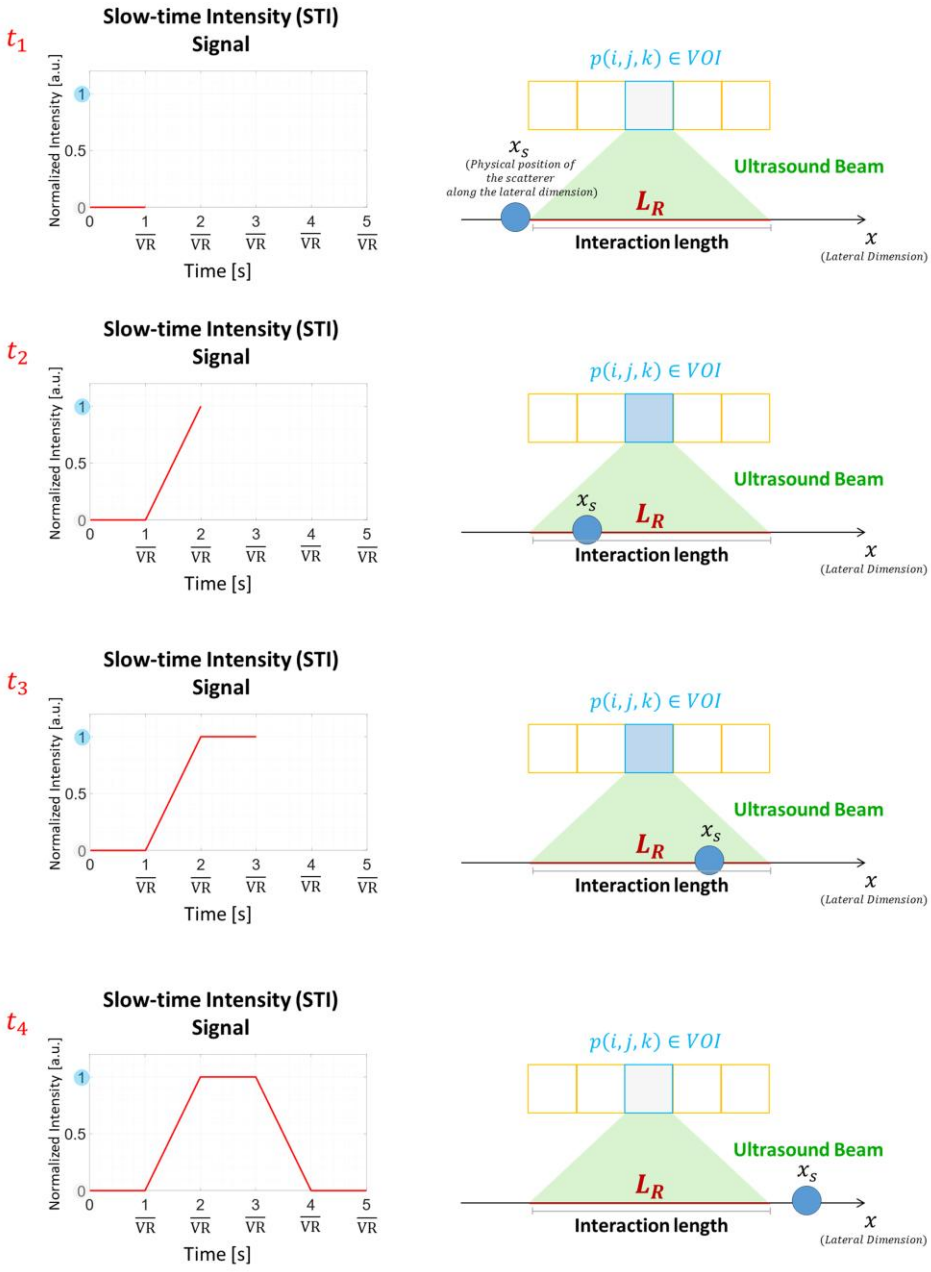

Figure 2. This figure illustrates the case of a moving scatterer (blue circle) influencing the intensity of a given pixel $\mathbf{p(i,j,k)}$ (highlighted in light blue). In this example, the pixel is depicted as two-dimensional (2D), for simplicity. As a consequence, the coordinate j (spatial component along elevation dimension) is fixed, in this example. Across four time instants (t_1, t_2, t_3, and t_4), the scatterer moves in space along the lateral dimension. In t_2 and t_3, the scatterer interacts with the ultrasound beam profile (light green area) and, therefore, influences the STI signal (plots in the left column). The spatial length of this interaction is determined by the ultrasound beam profile along lateral dimension, which is equal to the lateral resolution (L_R).

B. VELOCITY ESTIMATION

For each acquisition, a velocity model based on fUS was applied to estimate LSM velocity. The process workflow applied to the RF data acquired during NBr and FBr is illustrated in Figure 1. To further clarify, the processed RF data consist of a 4D matrix (one for NBr and one for FBr) composed of 200 volumes (2x2x5 cm volumes acquired at a frame rate of 40 Hz for 5 seconds). No upsampling was performed along slow time to

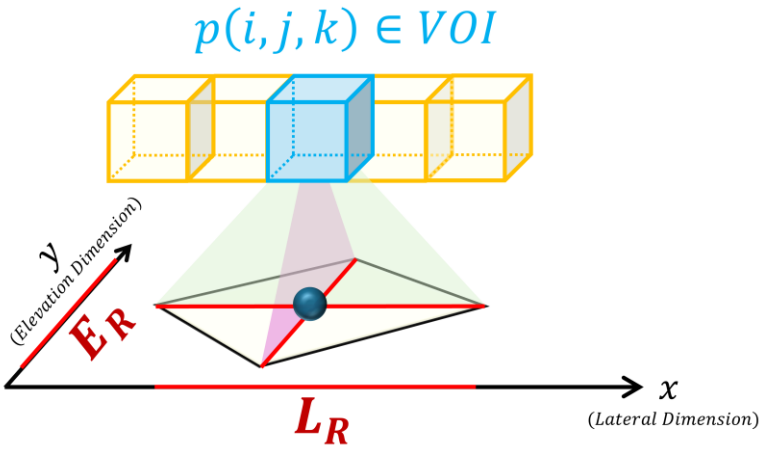

Figure 3. This figure illustrates the case of a moving scatterer (blue circle) influencing the intensity of a pixel $p(i,j,k)$ (highlighted in light blue) in 4D B-mode imaging. In this case, a scatterer has an influence on the STI signal when moving within the lateral and the elevation resolutions.

increase the number of frames, and no motion compensation approaches was applied to the RF data. The process applied to the RF is divided into the following five steps.

i) In the first step, the volume of interest (VOI) is defined as to totally include the PPl, i.e., from approximately 17 to 22 mm along depth and covering the entire lateral and elevation dimensions (see Figure 1.i).

Then, the velocity of each tridimensional (3D) pixel ($p(i,j,k)$) is estimated by implementing the second, third, and fourth steps for each 3D pixel.

ii) Specifically, the 200-points Fast Fourier Transform (FFT) of the slow-time intensity signal (STI) is computed in the second step (Figure 1.ii).

iii) Then, in the third step, the frequency at which the FFT shows the maximum magnitude (see Figure 1.iii) is selected as the pixel frequency ($f_{p(i,j,k)}$). To clarify, no specific separation criteria have been utilized when selecting the FFT peaks ($f_{p(i,j,k)}$ is only defined as the frequency at which the FFT shows the maximum magnitude).

iv) In the fourth step (Figure 1.iv), $f_{p(i,j,k)}$ is used to derive LSM velocity ($v_{p(i,j,k)}$) by implementing a velocity model based on fUS.

Specifically, the velocity model we developed considers the frequency content of STI signals to be correlated with the velocity of scatterers moving within the pixel field of view (FOV). The FOV is determined by the beam profile and, consequently, by the resolution. In 3D B-mode data (lateral dimension, axial dimension, and time), the lateral resolution determines the interaction length, which is the maximum length within which a moving scatter influences the STI signal (see Figure 2). To further clarify, we can consider the example depicted in Figure 2, where a moving scatterer is influencing the intensity of a given pixel $p(i,j,k)$. In this example, the pixel is depicted as two-dimensional (2D), for simplicity. As a consequence, in this example, the coordinate *j* (spatial component along elevation dimension) is fixed. We here assume a movement of the scatterer only along the lateral dimension, across four time instants (t_1, t_2, t_3, and t_4). Here it is also important to highlight how x_s is the physical position of the scatterer along the lateral dimension, whereas the index i indicates the pixel coordinate along the lateral dimension. At t_1 the scatterer is not intercepted by the ultrasound beam, thus the intensity would not change (it will remain 0 in this example). In t_2 and t_3, the scatterer interacts with the ultrasound beam profile (light green area in Figure 2) and, therefore, influences the STI signal (it will become 1, as shown in the left column of Figure 2). The spatial length of this interaction is determined by the ultrasound beam profile along lateral dimension, which is equal to the lateral resolution (L_R). In other words, the maximum spatial length that a scatterer can travel in the STI sampling interval and still have an influence on the STI signal is shown here to be equal to the lateral resolution (L_R). Finally, in t_4, the scatterer is not intercepted by the ultrasound beam anymore, thus the STI signal will go back to 0. As the same concept can be applied along the elevation dimension, in 4D data, the FOV is determined by both the lateral (L_R) and the elevation (E_R) resolutions, as shown in Figure 3. In this case,

the interaction length is defined as the maximum of the two resolution values. Indeed, given that the movement can be along the lateral or elevation dimensions, the maximum measurable velocity depends on the broadest (and, thus, worst) resolution between the lateral (L_R) and elevation (E_R) resolutions. However, it is important to clarify that this a simplified model, as the scatterer can potentially move along a direction that is a combination of the two dimensions (lateral and elevation). Moreover, as the imaging strategy is supposed to be symmetric, we theoretically would not expect differences in the two resolutions. However, as the experimental measurements of the resolution were performed considering a wire phantom [CIRS General Purpose Ultrasound Phantom (CIRS/Sun Nuclear, Norfolk, Virginia, USA)], which needed to be rotated of 90 degree to measure the two resolutions along the two orthogonal dimensions (i.e., lateral and elevation dimensions), these experimental measurements could lead to differences (300 µm at -6 dB, in this case) in the L_R and E_R. Therefore, to be consistent with the theoretical symmetry of the imaging strategy, we decided to compute the average between the two resolutions, to estimate the velocity. This average resulted to be 3.48 mm at -6 dB. Consequently, the velocity model to estimate LSM velocity is defined as follows

$$v_{p(i,j,k)} = \left(\frac{L_R + E_R}{2}\right) 2\, f_{p(i,j,k)} \quad \forall\, p(i,j,k) \in VOI \tag{1}$$

It is important to clarify that L_R and E_R were measured and estimated by using the same transmission/reception schemes (4-angle plane wave compounding) utilized to acquire the data from the volunteer. The resolutions were estimated with a wire phantom, and the wire's depth was approximately equal to the PPl depth (i.e., 20 mm). Given these premises, it is straightforward that the interaction length at a 20-mm depth can be approximated with the lateral (L_R) and elevation (E_R) resolutions of the system (given that the latter were measured by acquiring data from the wire phantom with the same transmission/reception schemes utilized to acquire the data from the volunteer). Theoretically, a plane wave imaging strategy with no compounding would lead to a wider beam and, according to equation (1), that would increase the capability of this approach to estimate higher velocities. Moreover, a plane wave imaging strategy with no compounding would allow the increase of the frame rate, thus allowing the estimation of even higher velocities. However, given that the highest velocity that we can estimate with the utilized 4-angle plane wave compounding acquisition strategy is already particularly high (139.20 mm/s) for LSM, we choose it to perform the acquisitions.

v) As a final step, the mean $v_{p(i,j,k)}$ is computed (Figure 1.v) for each case (NBr and FBr), to enable comparison.

3. RESULTS AND DISCUSSION

Figure 1 (row iv) illustrates the reconstructed volumes with each pixel color-coded according to its own velocity. The difference in color between the two volumes highlights the variations in LSM in the two cases. This difference is also reflected in the mean $v_{p(i,j,k)}$ values reported in Table 1. The mean $v_{p(i,j,k)}$ are 7.01 mm/s and 13.17 mm/s for NBr and FBr, respectively. The median $v_{p(i,j,k)}$ are 5.56 mm/s and 9.74 mm/s for NBr and FBr, respectively. By looking at the full distributions of the two velocity maps (Figure 4), it is clear how the two distributions are significantly different. Indeed, the Mann-Whitney U test[17] (performed with the *ranksum* MATLAB function) resulted in a p-value < 0.001. These values are consistent with the increase in breathing rate for FBr with respect to NBr, highlighting the potential of this methodology to detect physiological changes. Finally, the estimated velocities are within the physiological range, proving the possibility of estimating LSM velocities with 4D LUS.

Table 1. Estimated mean $v_{p(i,j,k)}$

Breathing type	**Breathing rate** [breaths/min]	**Mean $v_{p(i,j,k)}$** [mm/s]
NBr	$10-20$	7.01
FBr	$40-60$	13.17

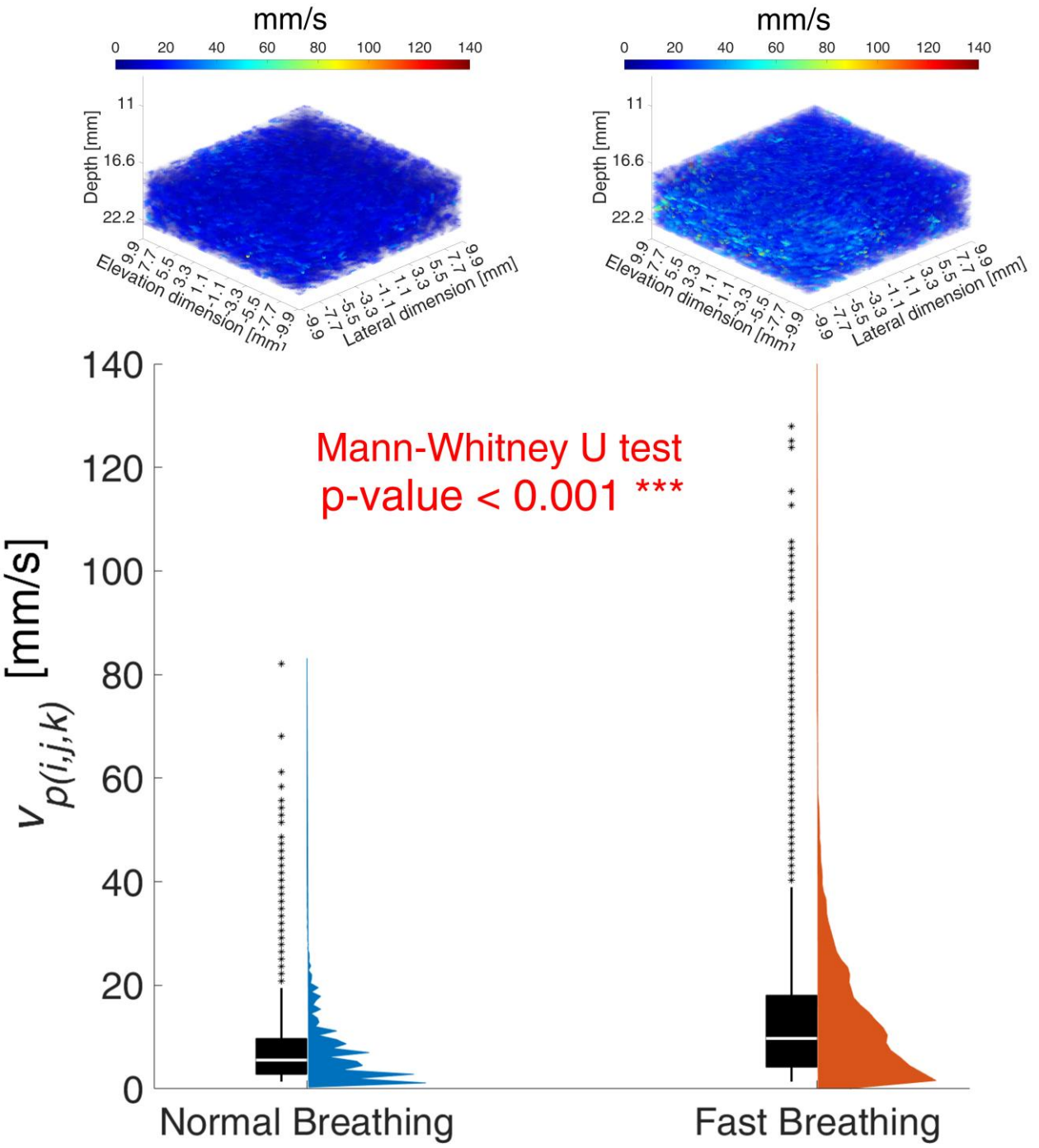

Figure 4. This figure shows the full distributions of the velocity maps obtained for Normal Breathing (NBr) [left] and Fast Breathing (FBr) [right]. On top, the obtained velocity maps are shown with a different colormap compared to the one used in Figure 1.iv. The dynamic range of the colormap is also different, to render it consistent with the daviolinplot[18] of the full distributions (bottom). The white lines on the daviolinplot[18] indicate the median values of the distributions.

4. CONCLUSION AND FUTURE WORK

In this study, we presented a new methodology to estimate the LSM velocity by applying a velocity model based on fUS to 4D LUS data. The use of 4D data potentially presents more reliable results with respect to the typical B-mode cross-sectional 3D data, as 4D data also include the elevation dimension. The results highlight

the ability of the methodology to estimate velocity within the physiological range and to detect variations in breathing. Despite this preliminary results demonstrated the validity of this work, we would like to highlight how this represents a feasibility study with only one volunteer. Future work will analyze a higher number of subjects to increase the robustness of the results. For example, data acquired from different scanning areas could report differences in LSM, as highlighted in previous studies[6,8,14]. Moreover, we plan to conduct experimental studies, in which the LSM velocity is controlled and known, to validate the proposed approach and compare its performance with more conventional motion estimation approaches (e.g., Kasai[16]). Finally, this methodology could be utilized to detect differences in velocity among different lung pathologies, potentially characterizing them. This could improve the clinical relevance of this methodology in the diagnosis of lung diseases.

DISCLOSURE OF CONFLICT OF INTEREST

The authors Ziewomit Klimonda, Piotr Jarosik, and Marcin Lewandowski are affiliated with us4us, a company developing and selling ultrasound scanners, included the one utilized in this research (us4R-lite™).

REFERENCES

[1] Mento, F., Khan, U., Faita, F., Smargiassi, A., Inchingolo, R., Perrone, T., and Demi, L. "State of the Art in Lung Ultrasound, Shifting from Qualitative to Quantitative Analyses," Ultrasound Med. Biol., **48**, 2398–2416. (**2022**). doi:https://doi.org/10.1016/j.ultrasmedbio.2022.07.007

[2] Demi, L., Wolfram, F., Klersy, C., De Silvestri, A., Ferretti, V. V., Muller, M., Miller, D., et al. "New International Guidelines and Consensus on the Use of Lung Ultrasound," J. Ultrasound Med., **42**, 309–344. (**2023**). doi:https://doi.org/10.1002/jum.16088

[3] Mento, F., Soldati, G., Prediletto, R., Demi, M., and Demi, L. "Quantitative Lung Ultrasound Spectroscopy Applied to the Diagnosis of Pulmonary Fibrosis: The First Clinical Study," IEEE Trans. Ultrason. Ferroelectr. Freq. Control, **67**, 2265–2273. (**2020**). doi:10.1109/TUFFC.2020.3012289

[4] Mento, F., Perpenti, M., Barcellona, G., Perrone, T., and Demi, L. "Lung Ultrasound Spectroscopy Applied to the Differential Diagnosis of Pulmonary Diseases: An In Vivo Multicenter Clinical Study," IEEE Trans. Ultrason. Ferroelectr. Freq. Control, **71**, 1217–1232. (**2024**). doi:10.1109/TUFFC.2024.3454956

[5] Perpenti, M., Mento, F., Pierro, G., Perrotta, A., Perrone, T., Smargiassi, A., Inchingolo, R., et al. "Fully automated Quantitative Lung Ultrasound spectroscopy for the differential diagnosis of lung diseases: The first multicenter in-vivo clinical study," Comput. Biol. Med., **200**, 111365. (**2026**). doi:https://doi.org/10.1016/j.compbiomed.2025.111365

[6] Inchingolo, R., Zanforlin, A., Buonsenso, D., Perrone, T., Torri, E., Limoli, G., Mossolani, E. E., et al. "Lung Ultrasound Signs," J. Ultrasound Med., **43**, 629–641. (**2024**). doi:https://doi.org/10.1002/jum.16397

[7] Lichtenstein, D. A., and Menu, Y. "A bedside ultrasound sign ruling out pneumothorax in the critically ill: Lung sliding," Chest, **108**, 1345–1348. (**1995**). doi:10.1378/chest.108.5.1345

[8] Briganti, D. N., Choi, C. E., Nguyen, J., and Lanks, C. W. "Determinants of point-of-care ultrasound lung sliding amplitude in mechanically ventilated patients," Ultrasound J., **15**, 25. (**2023**). doi:10.1186/s13089-023-00326-5

[9] Lichtenstein, D. A. "Lung Ultrasound (in the Critically Ill) Superior to CT: the Example of Lung Sliding.," Korean J. Crit. care Med., **32**, 1–8. (**2017**). doi:10.4266/kjccm.2016.00955

[10] Şirin, İ., Erdem, A. B., Uysal, Ş. B., and Gedikaslan, Ş. "The Effect of Tidal Volumes of Mechanically Ventilated Patients on Lung Sliding Amplitude in Point-Of-Care Lung Ultrasound," J. Clin. Ultrasound, **53**, 989–996. (**2025**). doi:https://doi.org/10.1002/jcu.23968

[11] Duclos, G., Marecal, L., Resseguier, N., Postzich, M., Taguet, C., Hraiech, S., Leone, M., et al. "Pleural lung sliding quantification using a speckle tracking technology: A feasibility study on 30 healthy volunteers," Comput. Methods Programs Biomed., **254**, 108316. (**2024**). doi:https://doi.org/10.1016/j.cmpb.2024.108316

[12] Duclos, G., Bobbia, X., Markarian, T., Muller, L., Cheyssac, C., Castillon, S., Resseguier, N., et al. "Speckle tracking quantification of lung sliding for the diagnosis of pneumothorax: a multicentric observational study," Intensive Care Med., **45**, 1212–1218. (**2019**). doi:10.1007/s00134-019-05710-1

[13] Fissore, E., Zieleskiewicz, L., Markarian, T., Muller, L., Duclos, G., Bourgoin, M., Michelet, P., et al. "Pneumothorax diagnosis with lung sliding quantification by speckle tracking: A prospective multicentric observational study," Am. J. Emerg. Med., **49**, 14–17. (**2021**). doi:https://doi.org/10.1016/j.ajem.2021.05.022

[14] Xiao, R., Shao, Q., Zhao, N., Liu, F., and Qian, K.-J. "Quantification analysis of pleural line movement for the

diagnosis of pneumothorax," World J. Clin. Cases, **9**, 5889–5899. (**2021**). doi:10.12998/wjcc.v9.i21.5889]

[15] Tzadok, B., Blumberg, Y., Shubert, M., Halabi, M., Tal-Or, E., Bachner-Hinenzon, N., and Carasso, S. "Speckled Tracking of Pleura—A Novel Tool for Lung Ultrasound; Distinguishing COVID-19 from Acute Heart Failure," J. Clin. Med., (**2022**). doi:10.3390/jcm11164846

[16] Kasai, C., Namekawa, K., Koyano, A., and Omoto, R. "Real-Time Two-Dimensional Blood Flow Imaging Using an Autocorrelation Technique," IEEE Trans. Sonics Ultrason., **32**, 458–464. (**1985**). doi:10.1109/T-SU.1985.31615

[17] Mann, H. B., and Whitney, D. R. "On a Test of Whether one of Two Random Variables is Stochastically Larger than the Other," Ann. Math. Stat., **18**, 50–60. (**1947**). Retrieved from https://doi.org/10.1214/aoms/1177730491

[18] Karvelis, P., Miyashita, T., and Oyvindlr "povilaskarvelis/DataViz: v3.2.7," (**2025**). Retrieved from https://doi.org/10.5281/zenodo.14614098